A monolithic multigrid solver for 3d fluid-structure interaction problems

T. Richter[†]

July 6, 2011

In this paper, we propose a geometric multigrid method for fluid-structure interaction problems in ALE coordinates. We aim at complex three dimensional systems describing the coupled dynamics of an incompressible fluid with an elastic structure. The equations in ALE formulation are discretized with stabilized finite elements on adaptively refined meshes.

The focus of this work is on the geometric multigrid method used to solve the linearized equations. Key is the construction of a smoothing operation based on a splitting of the problem into a fluid and structure part.

Besides analyzing the multigrid method, we will demonstrate the efficiency of the resulting solver on a complex three dimensional benchmark problem.

1 Introduction

In this work we present a geometric multigrid method for solving three dimensional fluid structure interaction problems in monolithic formulation. These kind of problems describe the interaction of an fluid (here incompressible and Newtonian) with an elastic structure.

Computational fluid mechanics and structure mechanics are two major areas of numerical simulation of physical systems. With the introduction of high performance computing it has become possible to tackle coupled systems with fluid and structure dynamics. General examples of such fluid-structure interaction (FSI) problems are flow transporting elastic particles (particulate flow), flow around elastic structures (e.g., airfoils) and flow in elastic structures (e.g., heart valves). In all these settings the dilemma in modeling the coupled dynamics is that the fluid model is normally based on an Eulerian perspective in contrast to the usual Lagrangian description of the solid model. This

[†]University of Heidelberg, Institute for Applied Mathematics, INF 293, 69120 Heidelberg, Germany, thomas.richter@iwr.uni-heidelberg.de

makes the setup of a common variational formulation difficult. However, such a variational formulation of FSI is needed as the basis of a consistent approach to residual-based a posteriori error estimation and mesh adaptation as well as to the solution of optimal control problems by the Euler-Lagrange method.

To achieve a closed variational formulation for the FSI problem, usually an auxiliary unknown coordinate transformation function T_f is introduced for the fluid domain. With its help the fluid problem is rewritten on the transformed domain. Then, all computations are done on the reference domain which is fixed in time. As part of the computation, the auxiliary transformation function T_f has to be determined at each time step. Such, so-called *arbitrary Lagrangian-Eulerian* (ALE) methods are described for instance in Huerta and Liu [21] or Wall [27].

Traditionally, fsi-problems are treated by *partitioned approaches*: In every time-step $t_{n-1} \to t_n$ of an outer iteration, the problem is split into the flow problem and into the structure problem. These problems are solved independently from each other in an iterative manner, while the interface-condition is considered via boundary conditions in an explicit manner. These partitioned schemes work well for large scale problems, e.g. in aeroelasticity, where the coupling is week, see Piperno and Farhat [23], they however fail to work efficiently, when the coupling gets strong. This is e.g. the case for applications in hemodynamics, where the ratio of fluid density to solid density is close to one (the *added mass effect*), see Causin, Gereau and Nobile [11].

The big advantage of partitioned approaches is that "Smaller and better conditioned subsystems are solved instead of one overall problem", see Förster, Wall and Ramm [13]. These subfields, fluid and structure can be treated with existing standard tools. Very efficient black-box solvers exist for both subproblems. The drawback of these methods is that many subiterations are necessary to reach convergence of the coupled problem in every time-step. For strongly coupled problems like in hemodynamics these iteration can even fail to converge, see various contributions in [9]. Further, Heil an co-workers [16] have stated that even for problems with weak coupling, monolithic solvers can be more efficient if good solvers exist. They develop efficient preconditioners for Krylov subspace methods which utilize existing subfield solvers.

Efficient multigrid solvers for FSI problems in a monolithic formulation are still rare. For two-dimensional problems Turek and co-workers [20] report good results with smoother of Vanka type, where local sub-problems are solved for smoothing. Subject of the present paper is to describe a geometric multigrid method for solving the coupled FSI problem. Instead of using the subfield solvers for preconditioning, we split the problem within the multigrid smoother. This stems from observations by Brummelen and co-workers [8], which have stated that partitioned solvers serve as perfect smoothers within a multigrid method. In their work, they have theoretically analyzed a specific fluid-structure interaction system, the panel-problem.

Outline of this paper is as follows. Section 2 ("Formulation") introduces the basic notation and we present the coupled ALE formulation of the fluid-structure interaction problem. Section 3 ("Discretization") describes the spatial finite element discretization. In Section 4 ("Multigrid Solver"), the geometric multigrid solver is presented. Section 5 ("Analysis") is devoted to the numerical examination and theoretical analysis of the

proposed solver. In Section 6 ("Numerical Examples") numerical examples show the feasibility and efficiency of the multigrid method and finally, the paper is closed by Section 7 ("Summary").

2 Formulation

We start by introducing some basic notation: let $\Omega \subset \mathbb{R}^3$ be an open domain with polyhedral boundary, split into Ω_f and Ω_s, both open polyhedral domains in $\mathbb{R}^3$ with $\bar{\Omega} = \bar{\Omega}_f \cup \bar{\Omega}_s$ and $\Omega_f \cap \Omega_s = \emptyset$. By $\Gamma_i := \bar{\Omega}_f \cap \bar{\Omega}_s$ we denote the *interface* between the two subdomains.

We split the boundaries of Ω_f and Ω_s into Dirichlet and Neumann boundaries: $\partial\Omega_f = \Gamma_f^D \cup \Gamma_f^N \cup \Gamma_i$ and $\partial\Omega_s = \Gamma_s^D \cup \Gamma_s^N \cup \Gamma_i$, respectively. For a Lebesgue measurable set $X \subset \mathbb{R}^3$, we denote by $L^2(X)$ the Lebesgue space of square-integrable functions on X equipped with the usual inner product and norm

$$(f,g)_X := \int_X fg \, dx, \quad \|f\|_X^2 = (f,f)_X,$$

respectively, and correspondingly for vector- and matrix-valued functions. Mostly the domain X will be Ω, in which case we will skip the domain index in products and norms. By $(\cdot,\cdot)_f$ and $(\cdot,\cdot)_s$ we denote the products on the fluid and structure domain, respectively. Further, by

$$\langle f,g\rangle_\Gamma := \int_\Gamma fg \, \mathrm{d}s,$$

we denote the L^2-inner product on a lower-dimensional manifold. Here Γ can be part of the domain's boundary $\partial\Omega$ or the interface between the two subdomains. By n_f and n_s we denote the out-bound unit-normal vectors on the boundary of Ω_f and Ω_s. The functions in $L^2(X)$ (with $X = \Omega$, $X = \Omega_f$, or $X = \Omega_s$) with first-order distributional derivatives in L_X make up the Sobolev space $H^1(X)$. Further, $H_0^1(X;\partial X^D) = \{v \in H^1(X) : v_{|\partial X^D} = 0\}$, where ∂X^D, is that part of the boundary ∂X at which Dirichlet boundary conditions are imposed, usually $\partial X^D = \Gamma^D$, $\partial X^D = \Gamma_f^D$ or $\partial X^D = \Gamma_s^D$.

In the context of fluid-structure interaction, we need to deal with moving domains. Under load, the subdomains will change: forces of the fluid will lead to a deformation of the obstacle $\Omega_s \to \Omega_s(t)$. This will hence give rise to a modification of the flow domain $\Omega_f \to \Omega_f(t)$ and a moved interface $\Gamma_i(t) = \bar{\Omega}_f(t) \cap \bar{\Omega}_s(t)$. In this work, we focus on the stationary case, where we are interested in the limit-configuration $\Omega \to \Omega_f(t_\infty)$ and $\Omega \to \Omega_s(t_\infty)$ only.

On the fluid domain $\Omega_s(t_\infty)$, the flow problem is described by the incompressible Navier-Stokes equations and on the solid domain $\Omega_s(t_\infty)$ we use an elastic material governed by the St. Venant Kirchhoff law. The loaded domain configuration $\Omega = \Omega_f(t_\infty) \cup \Omega_s(t_\infty)$ is a priori unknown and part of the problem's solution.

We use an ALE formulation (see [21] or [18] among many others) to model the fluid-structure interaction problems: the flow-domain $\Omega_f(t_\infty)$ is mapped to a reference flow

domain Ω_f via some mapping $T_f : \Omega_f \to \Omega_f(t_\infty)$. Likewise, the solid problem is formulated on the fixed Lagrangian structure domain Ω_s given by $T_s : \Omega_s \to \Omega_s(t_\infty)$. All computations are carried out on the fixed reference partitioning $\Omega = \Omega_f \cup \Omega_s$. The change of domains is implicitly taken care of by means of the transformations T_f and T_s. The dynamics of the coupled system is driven by the interface conditions asking for continuity of fluid's and solid's velocity as well as continuity of stresses across the interface Γ_i. The mapping $T_s : \Omega_s \to \Omega_s(t_\infty)$ is defined by the structural deformation u_s itself:

$$T_s(x,t) = x + u_s(x,t), \quad F_s := \nabla T_s = I + \nabla u_s, \quad J_s := \det(F_s).$$

We call F_s the deformation gradient. To define a mapping of the flow-domain we introduce the fluid's deformation u_f to define likewise

$$T_f(x,t) = x + u_f(x,t), \quad F_f := \nabla T_f = I + \nabla u_f, \quad J_f := \det(F_f).$$

In order for u_f to produce a feasible transformation, it must be an extension of u_s into the flow domain with $u_f = u_s$ on Γ_i. Several approaches exist for the definition of this ALE-mapping, see [12], here, we simply define u_f as an harmonic extension. In the following three subsections, we introduce both the fluid and solid problem as well as the fully coupled fluid-structure interaction problem.

2.1 The Fluid Problem

The principal variables describing the flow field are the velocity v_f, pressure p_f and deformation u_f.

The fluid problem is formulated as having Dirichlet boundary conditions $v_f = v_s$ on the interface Γ_i. The fluid deformation u_f is given as an harmonic extension of the solid's deformation u_s to Ω_f. Then, velocity, deformation and pressure are found in the spaces:

$$p_f \in L^2(\Omega_f), \quad v_f \in v_f^D + [H_0^1(\Omega_f; \Gamma_f^D)]^3, \quad u_f \in u_f^D + [H_0^1(\Omega_f; \partial\Omega_f)]^3,$$

where $v_f^D \in [H^1(\Omega_f)]^3$ is a suitable extensions of the Dirichlet values on $\Gamma_f^D := \Gamma_{\text{in}} \cup \Gamma_{\text{wall}} \cup \Gamma_i$ into the domain. While we allow an outflow condition for the velocity on Γ_{out} we use Dirichlet conditions for u_f on the complete boundary of Ω_f. If no outflow condition is present $\Gamma_{\text{out}} = \emptyset$, we restrict the pressure space to $L_0^2(\Omega_f) := L^2(\Omega)/\mathbb{R}$ in order to guarantee uniqueness of the solution.

The incompressible Navier-Stokes equations are mapped via T_f to Ω_f. See [12] for a complete derivation of the equations. The solution v_f, p_f, u_f is given by:

$$\begin{aligned} (\text{div}(J_f F_f^{-1} v_f), \xi)_f &= 0 \quad \forall \xi \in L^2(\Omega_f), \\ (J_f \rho_f F_f^{-T} v_f \cdot \nabla v_f, \phi)_f + (J_f \sigma_f F_f^{-T}, \nabla\phi)_f - \langle g_f^{\text{out}}, \phi \rangle_{\Gamma_{\text{out}}} &= 0 \quad \forall \phi \in [H_0^1(\Omega_f; \Gamma_f^D)]^3 \\ (\nabla u_f, \nabla \psi)_f &= 0 \quad \forall \psi \in [H_0^1(\Omega_f; \partial\Omega_f)]^3, \end{aligned} \tag{1}$$

where the stress-tensor transformed to ALE coordinates is given by

$$\sigma_f := -p_f I + \rho_f \nu_f (\nabla v F_f^{-1} + F_f^{-T} \nabla v_f^T), \tag{2}$$

with the fluid's density ρ_f and the kinematic viscosity ν_f. This formulation is well defined, as long as the ALE-mapping T_f is a C^2-diffeomorphism. For simplicity, external forces have been neglected. The boundary term on Γ_{out} is necessary to prevent spurious feedback of the *do-nothing* outflow condition, see [17], since using the full symmetric tensor is necessary when dealing with fsi-problems. g_f^{out} is given by:

$$g_f^{\text{out}} := n_f \cdot (J_f F_f^{-T} \nabla v_f^T F_f^{-T}). \tag{3}$$

2.2 The Structure Problem

The principal variables of the structure problem are the deformation u_s and the velocity v_s. For stationary problems we have $v_s = 0$ in Ω_s. The structure-problem is formulated as a Neumann-problem taking care of the continuity of stress-fluxes on Γ_i. We find u_s and v_s in the spaces

$$u_s \in [H_0^1(\Omega_s; \Gamma_s^D)]^3, \quad v_s \in [H_0^1(\Omega_s; \Gamma_s^D)]^3,$$

where we assumed for simplicity that only homogenous Dirichlet conditions are given on Γ_s^D for the solid's velocity and deformation. We find the solution as

$$\begin{aligned} (J_s \sigma_s F_s^{-T}, \phi)_s - \langle g_s^i, \phi \rangle_{\Gamma_i} = 0 \quad \forall \phi \in [H_0^1(\Omega_s; \Gamma_s^D)]^3, \\ (v_s, \psi)_f = 0 \quad \forall \psi \in [H_0^1(\Omega_s; \Gamma_s^D)]^3, \end{aligned} \tag{4}$$

with the solid's stress tensor given by

$$\sigma_s := 2\mu_s E_s + \lambda_s \text{tr}(E_s), \quad E_s := \frac{1}{2}(F_s^T F_s - I). \tag{5}$$

F_s is the deformation gradient as mentioned above, ρ_s the solid's density and λ_s and μ_s are the Lamé coefficients. On the interface Γ_i, g_s^i are the fluid's stresses given by

$$g_s^i := n_f \cdot (J_f \sigma_f F_f^{-T}). \tag{6}$$

2.3 The Fluid-Structure Interaction Problem

If both problems (1) and (4) are solved simultaneously, the coupled FSI problem is solved. The interface condition is taken care of by the Dirichlet-coupling $v_f = v_s$ as seen from the fluid-side and by the Neumann-condition $n_s \cdot (J_s \sigma_s F_s^{-T}) = n_f \cdot (J_f \sigma_f F_f^{-T})$ as seen from the structure side.

We combine these two problems into one monolithic formulation. To accommodate with the continuity of deformation and velocity across the interface, we search these variables as one common field in all Ω. Since there is no demand for continuity here, the pressure is extended with zero outside of Ω_f:

$$v \in v^D + [H_0^1(\Omega; \Gamma^D)]^3, \quad u \in [H_0^1(\Omega; \partial\Omega)]^3, \quad p \in L^2(\Omega_f)^{\text{ext}},$$

where $\Gamma^D := \Gamma_f^D \cup \Gamma_s^D$. Likewise, we define the transformation and its gradient on the whole domain Ω as

$$T := x + u, \quad F := \nabla T = I + \nabla u, \quad J := \det(F).$$

Then, the solution of the coupled fsi-problem is given by the set of equations:

$$\begin{aligned} (\mathrm{div}(JF^{-1}v), \xi)_f &= 0 \quad \forall \xi \in L^2(\Omega_f), \\ (\rho JF^{-T}v \cdot \nabla v, \phi)_f + (J\sigma_f F^{-T}, \nabla\phi)_f + (J\sigma_s F^{-T}, \nabla\phi)_s &= 0 \quad \forall \phi \in [H_0^1(\Omega; \Gamma^D)]^3, \\ (\nabla u, \nabla\psi)_f - \langle n_f \cdot \nabla u, \psi\rangle_{\Gamma_i} - (v, \xi)_s &= 0 \quad \forall \psi \in [H_0^1(\Omega; \partial\Omega)]^3, \end{aligned} \tag{7}$$

with the stress tensors defined as in (2) and (5). We have added the interface term in the ψ-equation to prevent spurious feedback from the implicit Neumann condition given due to integration by parts. While the continuity of velocity and deformation is included in the trial spaces, the continuity of stresses is guaranteed due to the boundary terms, implicitly given with integration by parts in the ϕ-equation.

3 Discretization

In this section, we detail the spatial discretization of the FSI problem based on its variational formulation. Our method of choice is the Galerkin finite element (FE) method with *conforming* finite elements. For a general introduction to the FE method, we refer to Carey and Oden [10], Girault & Raviart [14], Brenner & Scott [7], or Braess [6]. Having a Galerkin method for the completely discretized scheme at hand rigorous error estimation is accessible.

Let Ω_h be a triangulation of Ω, consisting of elements denoted by K,

$$\bar{\Omega} = \bigcup_{K \in \Omega_h} \bar{K},$$

which are (convex) hexahedrals in 3d. Such a decomposition Ω_h is referred to as *regular* if any element edge is either a subset of the domain boundary components, or a complete face or edge of another element. However, to facilitate mesh refinement and coarsening, we allow the elements to have a certain number of nodes that are at the midpoint of sides or faces of neighboring cells. These *hanging nodes* do not carry degrees of freedom and the corresponding function values are determined by linear or bilinear interpolation of neighboring *regular* nodal points. For more details on this construction, we refer to [10] or [5].

The mesh parameter h is a scalar cellwise constant function defined by $h|_K := h_K = \mathrm{diam}(K)$. We set $h_{\max} := \max_{K \in \Omega_h} h_K$. To ensure proper approximation properties of the finite element spaces which are constructed based on the meshes Ω_h, we require the *uniform-shape* condition to be fulfilled:

Mesh regularity condition: *Each element $K \in \Omega_h$ is the image of the reference unit cube $\hat{K} = [0,1]^d$ under some thee-linear mapping $T_K : \hat{K} \to K$. The Jacobian tensors*

∇T_K of these mappings are invertible and satisfy the uniform bounds

$$\sup_{h>0}\max_{K\in\Omega_h}\|h_K^{-1}\nabla T_K\|\le c,\qquad \sup_{h>0}\max_{K\in\Omega_h}\|h_K[\nabla T_K]^{-1}\|\le c. \tag{8}$$

This condition is satisfied if the elements $K\in\Omega_h$ possess the usual structural properties of uniform *non-degeneracy* and *uniform shape*. We however do not ask for an *uniform size property* to allow for local mesh refinement. The ratio of diameters h_K and $h_{K'}$ of different elements $K,K'\in\Omega_h$ does not need to be boundary for $h\to 0$.

In the context of fluid-structure interaction, we further assume, that no element K is cut by the interface: $K\cap\Gamma_i=\emptyset$ for all $K\in\Omega_h$. Hence, we can split the triangulation into two matching (up to hanging nodes on the interface) parts $\Omega_{h,f}$ and $\Omega_{h,s}$.

3.1 Finite element spaces

On Ω_h we introduce the usual space of isoparametric finite elements of order r by

$$V_h^{(r)}=\{\phi\in C(\bar\Omega),\ \phi\circ T_K^{-1}\in\operatorname{span}\{x^{\alpha_x}y^{\alpha_y}z^{\alpha_z},\ 0\le\alpha_x,\alpha_y,\alpha_z\le r\}, \tag{9}$$

where by $T_K:(0,1)^3\to K$ we indicate the mapping from the reference element onto the mesh element K. This mapping T_K itself is a polynomial of degree up to r (in every direction). We usually skip the superscript r if not especially required.

We introduce a basis $V_h=\operatorname{span}\{\phi_i,i=1,\dots,N\}$ of V_h by means of the usual nodal basis functions $\hat\phi_j$ on $\hat K=(0,1)^3$ and by transforming via $\phi^i|_K=\hat\phi_j\circ T_K^{-1}$. For all mesh-nodes $x_i\in\Omega_h$, we have $\phi_i(x_j)=\delta_{ij}$. On mesh nodes $x_i\in\Gamma^D$ on parts of the boundary where Dirichlet conditions are prescribed, we remove the corresponding nodal basis function from V_h, such that all functions in $V_h(\Omega;\Gamma_D)$ have trace zero on Γ^D.

The FSI problem (7) is then discretized by searching the solution in the discrete spaces. For pressure, velocity and deformation we use

$$p_h\in\mathcal{Q}_h,\ \mathcal{Q}_h:=V_h(\Omega),\quad v_h\in v_h^D+\mathcal{V}_h,\ \mathcal{V}_h:=[V_h(\Omega;\Gamma^D)]^3,\quad u_h\in\mathcal{W}_h,\ \mathcal{W}_h:=[V_h(\Omega;\partial\Omega)]^3.$$

The pressure is defined on all Ω and harmonically extended to Ω_s.

We combine $U_h:=(p_h,v_h,u_h)$ and $\Phi_h:=(\xi_h,\phi_h,\psi_h)$ and introduce the following semi-linear forms (linear in the second argument):

$$\begin{aligned}
a_f(U_h)(\Phi_h)&=(\operatorname{div}(JF^{-1}v_h),\xi_h)_f+(\rho JF^{-T}v_h\cdot\nabla v_h,\phi_h)_f\\
&\quad+(J\sigma_fF^{-T},\nabla\phi_h)_f-\langle n_f\cdot(J\sigma_fF^{-T}),\phi_h\rangle_{\Gamma_i}\\
&\quad+(\nabla u_h,\nabla\psi)_f-\langle n_f\cdot\nabla u_h,\psi\rangle_{\Gamma_i},\\
a_s(U_h)(\Phi_h)&=(J\sigma_sF^{-T},\nabla\phi_h)_s+\langle n_f\cdot(J\sigma_fF^{-T}),\phi_h\rangle_{\Gamma_i}\\
&\quad-(v_s,\psi_h)_s+(\nabla p_h,\nabla\xi_h)_s-\langle n_s\cdot\nabla p_h,\xi_h\rangle_{\Gamma_i},\\
a(U_h)(\Phi_h)&=a_f(U_h)(\Phi_h)+a_s(U_h)(\Phi_h).
\end{aligned} \tag{10}$$

The coupled fsi-problem is given by finding $U_h\in\mathcal{Q}_h\times v_h^D+\mathcal{V}_h\times\mathcal{W}_h$, such that

$$a(U_h)(\Phi_h)=0\quad\forall\Phi_h\in\mathcal{Q}_h\times\mathcal{V}_h\times\mathcal{W}_h. \tag{11}$$

In (10), the stress-coupling on the interface is artificially removed from the fluid-side and added to the structure side to elaborate the Dirichlet-Neumann coupling type of the problem. When solving the coupled equation like (11), this modification plays no role. It will however be important for deriving the multigrid solver.

These equal-order finite element spaces are not stable for discretizing incompressible flows, due to the lacking *inf-sup stability*. We use the *Local Projection Method* (LPS) for stabilizing the discretized equations, see [4] for an overview about LPS and [24] for an application to fsi-problems. In short, LPS works by adding certain stabilization terms to the semilinear-form $a_{\text{lps}}(\cdot)(\cdot)$ in order to control the fluctuations on the fines mesh level. The LPS method is also applicable to problems with dominant convection.

3.2 Solution of the nonlinear problems

The nonlinear problem (11) is solved with a Newton's method. Let $U_h^{(0)} \in v_h^D + \mathcal{V}_h$ be some initial guess (satisfying the boundary values). Then, the Newton iteration aim at finding updates $W_h^{(i)} \in \mathcal{V}_h$ such that:

$$i \geq 1: \quad U_h^{(i)} := U_h^{(i-1)} + W_h^{(i)}, \quad a'(U_h^{(i-1)})(W_h^{(i)}, \Phi_h) = -a(U_h^{(i-1)})(\Phi_h) \quad \forall \Phi_h \in \mathcal{V}_h. \tag{12}$$

Here, by $a'(U_h)(W_h, \Phi_h)$ we denote the directional derivative of the semilinear-form (10) at point U_h in direction W_h:

$$a'(U_h)(W_h, \Phi_h) := \frac{d}{ds} a(U_h + sW_h)(\Phi_h)\Big|_{s=0}.$$

While this *Jacobian* could be evaluated by means of finite differences or automatic differentiation, see [12], we analytically assemble the derivatives for reasons of numerical stability.

Focus of the present paper is the solution of the linear systems arising in every step of the Newton iteration (12). Hence, for the following considerations, we neglect all iteration indices regarding the nonlinear scheme. By introducing a nodal basis of the finite element space $\mathcal{Q}_h \times \mathcal{V}_h \times \mathcal{W}_h$,

$$\mathcal{Q}_h \times \mathcal{V}_h \times \mathcal{W}_h = \text{span}\{\Phi_h^i,\ i = 1, \ldots, N_{\text{dofs}}\}, \tag{13}$$

each step of (12) can be written in the compact matrix-formulation:

$$\mathbf{A}\mathbf{u} = \mathbf{b}, \tag{14}$$

where system matrix $\mathbf{A} \in \mathbb{R}^{N_{\text{dofs}} \times N_{\text{dofs}}}$ and load vector $\mathbf{b} \in \mathbb{R}^{N_{\text{dofs}}}$ are given by

$$(\mathbf{A})_{ij=1}^{N_{\text{dofs}}},\ \mathbf{A}_{ij} = a'(U_h)(\Phi_h^j, \Phi_h^i), \quad (\mathbf{b})_{i=1}^{N_{\text{dofs}}},\ \mathbf{b}_i = -a(U_h)(\Phi_h^j).$$

The system matrix $\mathbf{A}$ is usually very large $N_{\text{dofs}} \gg 100\,000$, it is however very dense, with only a fixed number of matrix entries (about 100 for 3d piece-wise quadratic finite elements) in every row.

4 Multigrid Solver

We aim at solving the linear system (14) by a geometric multigrid method using a hierarchy of locally refined meshes and finite element spaces. The basic outline of our multigrid method is presented in [2] and [22]. We assume, that coming from the fine mesh Ω_h, there exists a hierarchy of finite element meshes and spaces:

$$\Omega_h = \Omega_L \supset \Omega_{L-1} \supset \cdots \supset \Omega_0, \quad V_h = V_L \supset V_{L-1} \supset \cdots \supset V_0.$$

Every mesh Ω_l, $l = 0, \ldots, L$ in this hierarchy covers the whole domain and includes the fluid-structure coupling. On every mesh-level Ω_l, by $\mathbf{A}_l$ we denote the system matrix. The geometric multigrid approach is standard, see [15], and the unknown solution $\mathbf{u} \in \mathbf{R}^{N_{\text{dof}}}$ on the finest mesh Ω_h is approximated by Algorithm 1:

Algorithm 1: Geometric multigrid
Solve $\mathbf{A}\mathbf{u} = \mathbf{b}$. Given $\mathbf{A}_l$, $l = 0, \ldots, L$, $\mathbf{b}_L$ and an initial guess $\mathbf{u}_l^{(0)}$. For $i \geq 1$ iterate:

$$u^{(i+1)} = \mathbf{MG}(\mathbf{A}_l, \mathbf{u}_l^{(i)}, \mathbf{b}_l),$$

$\mathbf{MG}(\mathbf{A}_l, \mathbf{u}_l, \mathbf{b}_l)$		
if $l = 0$:	1. solve exact	$\mathbf{u}_0 = [\mathbf{A}_0]^{-1}\mathbf{b}_0$
if $l > 0$:	1. smooth	$\mathbf{u}_l^1 = \mathbf{SMOOTH}(\mathbf{u}_l; \mathbf{A}_l, \mathbf{b}_l)$
	2. residual	$\mathbf{r}_l = \mathbf{b}_l - \mathbf{A}_l\mathbf{u}_l^1$
	3. restrict	$\mathbf{r}_{l-1} = \mathcal{R}_{l-1}\mathbf{r}_l$
	4. coarse mesh	$\mathbf{u}_{l-1}^2 = MG(0; \mathbf{A}_{l-1}, \mathbf{r}_{l-1})$
	5. update	$\mathbf{u}_l^2 = \mathbf{u}_l^1 + \mathcal{P}_{l-1}\mathbf{u}_{l-1}^2$
	6. smooth	$\mathbf{u}_l^3 = \mathbf{SMOOTH}(\mathbf{u}_l^2; \mathbf{A}_l, \mathbf{b}_l)$
		return $\mathbf{u}_l^3$

This algorithm is the V-cycle of the standard geometric multigrid solver with pre- and post-smoothing in Steps 1. and 6. In Step 4., the multigrid solver is invoked recursively to approximate/solve the problem on the next coarse mesh. To improve the convergence and stability of the multigrid solver, this algorithm is usually taken as preconditioner in an outer Krylow subspace method. We use the multigrid to precondition a *GMRES* iteration.

Success of the multigrid solver heavily depends on the method used for smoothing. For simple problems like the Laplace equation very easy iterations like SSOR or Jacobi will suit as perfect smoothers. Considering saddle-point systems like coming from the incompressible Navier-Stokes equations, the problem of finding a suitable smoother gets larger. Here, mostly iterations of Vanka-type are taken. E.g. Turek and co-workers [20, 26], local subproblems coupling pressure and velocity are solved for smoothing. This method is reliable for difficult systems as visco-elasticity and complex flow problems. Good results have been reported for two dimensional FSI problems. Our approach is to use a block-incomplete LU decomposition of the matrices $\mathbf{A}_l$ as smoother. This is

comparable to Vanka-type solvers, with smaller blocks but stronger outer coupling, see Kimmritz and Richter [22] for the application to reactive flow and complex ocean flow problems. This smoother however fails for fluid-structure interaction problems. In this work, we will adapt this block-ILU smoother to take advantage of a splitting of the FSI-problem into a fluid and structure part.

In the following Section 4.1 we first introduce a special block-structure for the linear system. Then, in Section 4.2 we present the splitting approach used as smoother in Steps 1. and 6. of Algorithm 1.

4.1 Linear system with local block-structure

We introduce a local block-structure of the linear system (14). Here, we utilize the fact, that only equal-order finite elements are considered, where the same nodal basis is given for pressure, velocity and deformation. Hence, we can sort the basis (13) by clustering all degrees of freedom in the mesh-nodes:

$$\mathcal{Q}_h \times \mathcal{V}_h \times \mathcal{W}_h = \left\{\Phi_1^1, \Phi_1^2, \dots, \Phi_1^7,\ \Phi_2^1, \dots, \Phi_2^7,\ \dots\ \Phi_N^1, \dots, \Phi_N^7\right\},$$

where N is the number of mesh-nodes in Ω_h. 7 is the number of *solution components*: pressure, three velocities and deformations are given in the first node, followed by pressure, velocities and deformations in the second node, and so on. The total number of unknowns is $N_{\text{dof}} = 7N$. With this ordering of the unknowns, we obtain a local block-matrix:

$$(\mathbf{A}_{ij})_{c,d=1}^{7}, \quad \mathbf{A}_{ij}^{cd} = a(U_h)(\Phi_j^d, \Phi_i^c), \quad i,j = 1, \dots, N,$$

with the local matrix-blocks $\mathbf{A}_{ij} \in \mathbf{R}^{7\times 7}$. Likewise, we write every solution vector as

$$U_h = \sum_{i=1}^{N} \sum_{c=1}^{7} \mathbf{u}_i^c \Phi_i^c, \quad \mathbf{u}_i \in \mathbf{R}^7.$$

We call this matrix (in the specific ordering of unknowns) to be in block-form since all couplings between the different unknowns in one mesh-node are clustered. By $\mathbf{A}_{ij} \in \mathbb{R}^{7\times 7}$ we denote the local matrix blocks which contain all couplings between the 7 unknowns in nodes i and j. All linear algebra routines will work on this block-form, e.g. when computing an incomplete LU decomposition of the matrix $\mathbf{A}$, it will be a block-ILU, where each matrix block $\mathbf{A}_{ij} \in \mathbb{R}^{7\times 7}$ is inverted exactly, see [22]. One obvious advantage of this blocking is, that all linear algebra routines can be written independent on the size of the partial differential equation system, whether a scalar Laplacian or a four-component Navier-Stokes system. Further, for large systems of PDE's (like the seven solution components of the FSI problem) good cache efficiency is given for free. The main advantage however is, that by clustering the couplings in mesh-nodes, all routines are easily written as variants of the Vanka method.

By using the multigrid Algorithm 1. with a block-ILU smoother based on these matrix-blocks, a huge variety of complex flow problems can be tackled, see [22]. Fluid-structure interaction problems however still cannot be robustly solved by this multigrid scheme.

4.2 Definition of the splitting-preconditioner

In the following Section 5.1 we find evidence, that standard schemes fail to work on fluid-structure interaction problems due to the very bad conditioning of the system matrices. This conditioning however is introduced not by the difficulty of the two subproblems fluid and solid – which the block-ILU-smoother introduced above is able to solve very efficiently – but by the coupling of these two problems.

To take advantage of the existing methods for problems in fluid- and structure-dynamics, we introduce a splitting-approach within the multigrid smoother. The basic idea is to use a preconditioned Richardson iteration for smoothing in Steps 1. and 6. of the multigrid algorithm:

$$i \geq 1, \quad \mathbf{u}^{(i)} = \mathbf{u}^{i-1} + \mathbf{P}^{-1}\big(\mathbf{b} - \mathbf{A}\mathbf{u}^{(i-1)}\big), \tag{15}$$

where $\mathbf{P}$ is the preconditioner. This preconditioner consists of separately solving the fluid $\mathbf{F}$ and solid problem $\mathbf{S}$, in short:

$$\mathbf{u}^{(i)} = \mathbf{u}^{i-1} + \big([\mathbf{F}]^{-1} + [\mathbf{S}]^{-1}\big)\big(\mathbf{b} - \mathbf{A}\mathbf{u}^{(i-1)}\big).$$

We need some further notation: let $\mathcal{N}$ by the set of mesh-nodes, $\mathcal{N}_f$ the mesh-nodes entirely in the fluid-domain, $\mathcal{N}_i$ the nodes on the interface and $\mathcal{N}_s$ the solid-nodes. With $N := \#\mathcal{N}$, $N_f := \#\mathcal{N}_f$ $N_i := \#\mathcal{N}_i$ and $N_s := \#\mathcal{N}_s$ it holds $N = N_f + N_s + N + N_i = N_{\text{dofs}}/7$. By $\mathcal{R}_f$, $\mathcal{R}_s$ and $\mathcal{R}_i$ we denote the node-wise restriction of Ω_h to the set of sub-nodes and by $\mathcal{P}_f$, $\mathcal{P}_i$ and $\mathcal{P}_s$ we denote the corresponding prolongation operators.

Next, by $\mathbf{F} \in \mathbb{R}^{N_f^2 \cdot 7^2}$ and $\mathbf{S} \in \mathbb{R}^{(N_s+N_i)^2 \cdot 7^2}$ we denote the local matrices generated by restricting $\mathbf{A}$ to the fluid nodes $\mathbf{F}$ and to the solid and interface nodes $\mathbf{S}$ only. Note, that $\mathbf{A} \neq \mathbf{F} + \mathbf{S}$, since the couplings $i \leftrightarrow j$ with $i \in \mathcal{N}_f$ and $j \in \mathcal{N}_s \cup \mathcal{N}_i$ between the two different subsets are neglected. Further note, that the solid matrix $\mathbf{S}$ includes the interface nodes. This will be of importance to reflect the Dirichlet-Neumann coupling of the problem. Both local matrices have the block-form discussed above, and each block can be written as:

$$i,j \in \mathcal{N}_f : \ \mathbf{F}_{ij} = \begin{bmatrix} \mathbf{F}_{pp} & \mathbf{F}_{pv} & \mathbf{F}_{pu} \\ \mathbf{F}_{pv} & \mathbf{F}_{vv} & \mathbf{F}_{vu} \\ 0 & 0 & \mathbf{F}_{uu} \end{bmatrix} \qquad i,j \in \mathcal{N}_s : \ \mathbf{S}_{ij} = \begin{bmatrix} \mathbf{S}_{pp} & 0 & 0 \\ 0 & 0 & \mathbf{S}_{vu} \\ 0 & \mathbf{S}_{uv} & 0 \end{bmatrix}$$

The matrices $\mathbf{F}_{pp}, \mathbf{F}_{pv}, \mathbf{F}_{vp}, \mathbf{F}_{vv}$ assemble the Navier-Stokes system. In $\mathbf{F}_{pu}$ and $\mathbf{F}_{vu}$ the coupling to the ALE-mapping is given. The matrix $\mathbf{F}_{uu}$ is the discretization of the deformation's extension to the fluid domain. Likewise, by $\mathbf{S}_{pp}$ we denote the extension of the pressure to the structure domain. In $\mathbf{S}_{vu}$ the main part of the structure's equation and by $\mathbf{S}_{uv}$ the velocity equals zero condition is given.

Matrix entries belonging to interface test-functions have a different structure since on the interface Γ_i both equations are present. Here, we extend the fluid-system $\mathbf{F}$ to have Dirichlet-boundary values for velocity and deformation on Γ_i. On the structure-side, the interface includes the Neumann-condition of the fluid-tensor, see (6):

$$x_i \in \Gamma_i : \quad \mathbf{F}_{ii}^{\Gamma} = \begin{bmatrix} \mathbf{F}_{pp} & 0 & 0 \\ 0 & \mathbf{1} & 0 \\ 0 & 0 & \mathbf{1} \end{bmatrix} \qquad \mathbf{S}_{ii}^{\Gamma} = \begin{bmatrix} \mathbf{1} & 0 & 0 \\ 0 & \mathbf{F}_{vv} & \mathbf{S}_{vu} + \mathbf{F}_{vu} \\ 0 & \mathbf{S}_{uv} & 0 \end{bmatrix}$$

These modified matrices are again denoted by $\mathbf{F}$ and $\mathbf{S}$.

Remark: By introducing Dirichlet boundary values in the fluid-part of the preconditioner, the update of velocity and deformation will only be determined from the solid part. This is obviously the right choice for the deformation, since this is only to be considered as an artificial extension on the fluid domain.

These two sub-matrices are used to define the preconditioner of the Richardson iteration (15). In every step of the smoothing process, two subproblems need to be solved:

Algorithm 2: Smoothing iteration
Smooth $\mathbf{Au} = \mathbf{b}$. Given $\mathbf{A}$, $\mathbf{b}$, $\mathbf{F}$, $\mathbf{S}$ Given $\mathbf{A}_l$, $l = 0, \ldots, L$, $\mathbf{b}_L$ and an initial guess $\mathbf{u}_l^{(0)}$. For $i \geq 1$ iterate:

1. residual	$\mathbf{r}^{(i)} = \mathbf{b} - \mathbf{Au}^{(i-1)}$	
2. fluid problem	$\mathbf{Fw}_f^{(i)} = \mathcal{R}_f \mathbf{r}^{(i)}$	
3. update fluid	$\mathbf{u}^{(i)} = \mathbf{u}^{(i-1)} + \mathcal{P}_f \mathbf{w}_f^{(i)}$	
4. residual	$\mathbf{r}^{(i)} = \mathbf{b} - \mathbf{Au}^{(i-1)}$	(for Gauss-Seidel coupling)
5. solid problem	$\mathbf{Sw}_s^{(i)} = \mathcal{R}_s \mathbf{r}^{(i)}$	
6. update solid	$\mathbf{u}^{(i)} = \mathbf{u}^{(i)} + \mathcal{P}_s \mathbf{w}_s^{(i)}$	

Remark: In Steps 2. and 5., the subproblems are not to be solved exactly. Instead, at this point we apply the standard block-ILU-iteration for approximating the fluid and structure problem.

The structure of this smoother is very similar to a non-overlapping domain decomposition method with a Dirichlet-Neumann coupling. There is however the wide difference, that varying equations are given on the different domains.

5 Analysis

This section aims at analyzing the multigrid smoother developed before. In view of the lack of theoretical results for monolithic fluid-structure interaction problems, this task is very difficult. We split the investigation into two parts: first, we gather numerical evidence which supports the splitting approach by regarding the full nonlinear ALE model of the FSI problem. Then, we aim at analyzing the coupling strategy used within the multigrid smoother. Here, we consider a considerably simplified linear model-problem which however still includes the specific fluid-structure coupling at the interface.

5.1 Numerical observation

A straightforward geometric multigrid-iteration used as preconditioner in an outer GMRES iteration applied to the coupled fsi-problem fails to converge on finer meshes. In Table 1 we show convergence rates, obtained for the stationary two dimensional *fsi-1* FSI benchmark problem introduced by Hron and Turek [19]. The system is solved with

the geometric multigrid method as preconditioner in an outer GMRES iteration. We use 4 steps of the block-ILU iteration for pre- and post-smoothing of the coupled problem. The coarse mesh problem is solved by a direct solver. In Table 1, we present the convergence rates of the solver on a sequence of uniformly refined meshes and indicate the number of steps necessary to reduce the error by 10^6. On the finest mesh, the desired error reduction could not be reached within 50 steps. We see, that the convergence rates deteriorate and the number of steps necessary increases. This standard multigrid solver is thus not efficient.

levels	# elements	reduction rate	steps
1	248	< 0.00	1
2	992	0.09	7
3	3 968	0.24	13
4	15 872	0.45	19
5	63 488	0.63	32
6	254 952	0.91	> 50

Table 1: Convergence rates of the coupled multigrid iteration for the 2d fsi-1 benchmark problem.

We believe, that the bad convergence rates of the multigrid solver stems from the condition numbers of the system matrix which causes coupled smoothers to fail on large meshes. In Table 2 we list the numerically estimated condition numbers $\text{cond}_2(\mathbf{A})$ for the entire system matrix $\mathbf{A}$ as well as for the all sub-matrices which play a role in the splitting-smoother from Section 4.2: these are the Navier-Stokes part of the fluid-matrix $\mathbf{F}_{NS}$, the deformation part in the fluid-matrix $\mathbf{F}_{uu}$, the pressure part in the structure-system $\mathbf{S}_{pp}$ and the elastic-structure part $\mathbf{S}_{ES}$.

#elements	$\text{cond}_2(\mathbf{A})$	$\text{cond}_2(\mathbf{F}_{NS})$	$\text{cond}_2(\mathbf{F}_{uu})$	$\text{cond}_2(\mathbf{S}_{ES})$	$\text{cond}_2(\mathbf{S}_{pp})$
248	$4.77 \cdot 10^{10}$	$8.64 \cdot 10^{5}$	$7.40 \cdot 10^{1}$	$9.27 \cdot 10^{6}$	$1.26 \cdot 10^{1}$
992	$1.47 \cdot 10^{11}$	$1.54 \cdot 10^{6}$	$4.12 \cdot 10^{2}$	$9.27 \cdot 10^{6}$	$7.76 \cdot 10^{1}$
3 968	$5.06 \cdot 10^{11}$	$2.99 \cdot 10^{6}$	$1.66 \cdot 10^{3}$	$9.27 \cdot 10^{6}$	$2.69 \cdot 10^{2}$
15 872	$1.97 \cdot 10^{12}$	$7.91 \cdot 10^{6}$	$6.68 \cdot 10^{3}$	$9.27 \cdot 10^{6}$	$9.95 \cdot 10^{2}$
63 488	$7.84 \cdot 10^{12}$	$2.35 \cdot 10^{7}$	$2.68 \cdot 10^{4}$	$9.27 \cdot 10^{6}$	$3.81 \cdot 10^{3}$

Table 2: Condition numbers for the system matrix and the sub-matrices on a sequence of meshes. fsi-1 benchmark configuration.

The condition number of the coupled matrix $\mathbf{A}$ is much worse than that of the sub-matrices. Here, on finer meshes, an ILU-iteration as smoother fails due to numerical error accumulation. The conditioning of the subsystems is within reasonable limits and the standard multigrid iteration is able to solve these systems.

In Table 3 we show convergence results of the multigrid-method, where we use the splitting approach for the smoother but solve the two subsystems for the fluid and

solid problem in Steps 2. and 5. of Algorithm 2. with an exact solver. Here, the convergence rates are exceptionally good and do not worsen on finer meshes. This result is in analogy to Brummelen and co-workers [8], where it is shown, that the partitioned approach together with a coarse mesh correction is a perfect smoother for the panel problem.

levels	# elements	reduction rate	steps
1	248	< 0.01	1
2	992	< 0.01	2
3	3 968	< 0.01	2
4	15 872	< 0.01	2
5	63 488	< 0.01	2
6	254 952	< 0.01	2

Table 3: Convergence rates for a standard geometric multigrid iteration on the coupled fsi-problem. All reduction rates are smaller than 0.01.

Hence, we can conclude, that the partitioned smoother is suitable for the multigrid iteration, if the two subproblems for fluid and solid are approximated up to a sufficient accuracy. Since the condition numbers of these subproblems is within limits, standard methods like block-ILU iterations will be feasible for treating the fluid and structure problem.

5.2 Analysis of a simplified model problem

Next, we aim at analyzing the coupling between the fluid and structure problem in detail. For a better understanding we considerably simplify the fluid-structure interaction model:

- We omit all nonlinearities (convection, domain-deformation, nonlinear elasticity)
- We use the Laplacian as fluid and structure tensor
- We remove the divergence condition and the pressure
- We use a scalar field for velocity and deformation

The complete simplified model states: find "velocity" and "deformation" v and u such that:

$$\left.\begin{aligned} -\Delta v_f &= f \\ -\Delta u_f &= 0 \end{aligned}\right\} \text{ in } \Omega_f, \qquad \left.\begin{aligned} -\Delta u_s &= f \\ -v_s &= 0 \end{aligned}\right\} \text{ in } \Omega_s, \qquad \left.\begin{aligned} v_f &= u_s \\ n \cdot \nabla v_f &= n \cdot \nabla u_s \end{aligned}\right\} \text{ on } \Gamma_i.$$

The monolithic variational formulation is derived by finding "velocity" and "deformation" in the spaces $u, v \in H_0^1(\Omega)$, given by

$$(\nabla v, \nabla \phi)_f + (\nabla u, \nabla \phi)_s + (\nabla u, \nabla \psi)_f - \langle n_f \cdot \nabla u, \psi \rangle_{\Gamma_i} - (v, \psi)_s = (f, \phi) \quad \forall \phi, \psi \in H_0^1(\Omega). \quad (16)$$

We consider the domain $\Omega = (0,2) \times (0,1)$ split into $\Omega_f = (0,1) \times (0,1)$ and $\Omega_s = (1,2) \times (0,1)$. Let Ω_h be a uniform triangulation of Ω with mesh-size h. Further, let V_h be the finite element space of piecewise bi-linear function on Ω_h. By splitting the nodes of Ω_h into the fluid-nodes $\mathcal{N}_f$, the interface nodes $\mathcal{N}_i$ and the solid nodes $\mathcal{N}_s$, see Section 4.2, the linear system (16) is equivalent to finding $\mathbf{x} = \{\mathbf{v}_f, \mathbf{u}_f, \mathbf{v}_i, \mathbf{u}_i, \mathbf{v}_s, \mathbf{u}_s\}$, given by:

$$\left(\begin{array}{cc|cc|cc} \Delta & 0 & \Delta & 0 & 0 & 0 \\ 0 & \Delta & 0 & \Delta & 0 & 0 \\ \hline \Delta & 0 & \Delta & \Delta & 0 & \Delta \\ 0 & \mathbf{0} & -1 & \mathbf{0} & -1 & 0 \\ \hline 0 & 0 & 0 & \Delta & 0 & \Delta \\ 0 & 0 & -1 & 0 & -1 & 0 \end{array}\right) \left(\begin{array}{c} v_f \\ u_f \\ \hline v_i \\ u_i \\ \hline v_s \\ u_s \end{array}\right) = \mathbf{b}, \tag{17}$$

where Δ stands for the discretization of the Laplacian, -1 for the (lumped) mass matrix. The bold zeros arise from the subtracted boundary term in the fluid's deformation extension equation in (16).

Remark: The off-diagonal entries are to be understood in a symbolic way: not all fluid-nodes in the first row of (17) couple to the interface nodes v_i, only those next to the interface. These off-diagonal blocks are thus very sparse.

The preconditioner of the fluid problem is constructed to have Dirichlet conditions for velocity and deformation on the interface. Hence, the interface unknowns do not couple back to the flow-block. The structure part of the preconditioner is generated by restricting (17) to the structure and interface nodes.

We aim at analyzing the error before $\mathbf{e}^{(i-1)} = \mathbf{x} - \mathbf{x}^{(i-1)}$ and after $\mathbf{e}^{(i)} = \mathbf{x} - \mathbf{x}^{(i)}$ one step of the smoothing iteration, Algorithm 2. With (15), the error is related by

$$\mathbf{e}^{(i)} = \mathbf{x} - \mathbf{x}^{(i)} = \mathbf{e}^{(i-1)} - \mathbf{P}^{-1}(\mathbf{b} - \mathbf{A}\mathbf{x}^{(i-1)}) = [I - \mathbf{P}^{-1}\mathbf{A}]\mathbf{e}^{(i-1)}.$$

Depending on whether a Jacobi or Gauss-Seidel iteration is used for preconditioning, $\mathbf{P}$ is given as:

$$\mathbf{P}_J = \left(\begin{array}{cc|cc|cc} \Delta & 0 & 0 & 0 & 0 & 0 \\ 0 & \Delta & 0 & 0 & 0 & 0 \\ \hline 0 & 0 & \Delta & \Delta & 0 & \Delta \\ 0 & 0 & -1 & 0 & -1 & 0 \\ \hline 0 & 0 & 0 & \Delta & 0 & \Delta \\ 0 & 0 & -1 & 0 & -1 & 0 \end{array}\right), \quad \mathbf{P}_{GS} = \left(\begin{array}{cc|cc|cc} \Delta & 0 & 0 & 0 & 0 & 0 \\ 0 & \Delta & 0 & 0 & 0 & 0 \\ \hline \Delta & 0 & \Delta & \Delta & 0 & \Delta \\ 0 & 0 & -1 & 0 & -1 & 0 \\ \hline 0 & 0 & 0 & \Delta & 0 & \Delta \\ 0 & 0 & -1 & 0 & -1 & 0 \end{array}\right),$$

with differences only whether the solid system couples back to the already computed fluid-update. For simplicity we introduce the shorter notation, combining the interface and solid nodes $\mathcal{N}_S := \mathcal{N}_i \cup \mathcal{N}_s$:

$$\mathbf{A} = \left(\begin{array}{cc} \mathbf{F} & \mathbf{FS} \\ \mathbf{SF} & \mathbf{S} \end{array}\right), \quad \mathbf{P}_J^{-1} = \left(\begin{array}{cc} \mathbf{F}^{-1} & 0 \\ 0 & \mathbf{S}^{-1} \end{array}\right), \quad \mathbf{P}_{GS}^{-1} = \left(\begin{array}{cc} \mathbf{F}^{-1} & 0 \\ -\mathbf{S}^{-1}[\mathbf{SF}]\mathbf{F}^{-1} & \mathbf{S}^{-1} \end{array}\right).$$

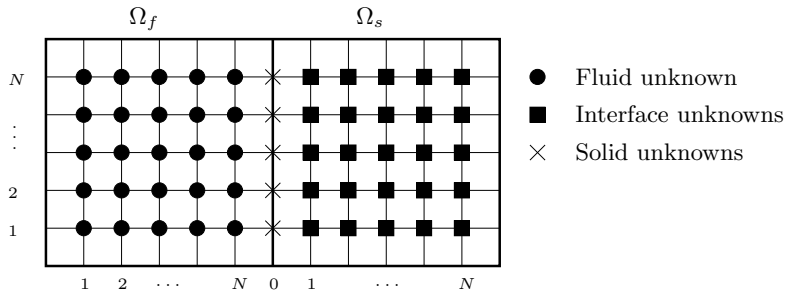

Figure 1: Domain layout for the simplified analysis.

Then, one iteration of the smoother alters the error by $\mathbf{e}^{(i)} = [I - \mathbf{P}^{-1}\mathbf{A}]\mathbf{e}^{(i-1)}$ with:

$$[I - \mathbf{P}_J^{-1}\mathbf{A}] = \begin{pmatrix} 0 & -\mathbf{F}^{-1}[\mathbf{FS}] \\ -\mathbf{S}^{-1}[\mathbf{SF}] & 0 \end{pmatrix}, \quad [I - \mathbf{P}_{GS}^{-1}\mathbf{A}] = \begin{pmatrix} 0 & -\mathbf{F}^{-1}[\mathbf{FS}] \\ 0 & -\mathbf{S}^{-1}[\mathbf{SF}]\mathbf{F}^{-1}[\mathbf{FS}] \end{pmatrix}$$

Remark: Note, that for now we assume, that the subproblems are solved exactly. The inversion of $\mathbf{F}$ and $\mathbf{S}$ needs to be replaced by a suitable approximation. We will give further hints on this.

We perform a Fourier analysis of the error for a better insight in the smoothing iteration. On the uniform mesh as shown in Figure 1 we introduce Fourier components:

Definition 5.1 (Fourier Components)**.** *For $\theta = 1, \ldots, N$ we define the Dirichlet components Φ_θ^D*

$$\Phi_\theta^D = \sin\left(\frac{i}{N+1}\theta\pi\right), \quad i = 1, \ldots, N,$$

and for $\theta = 0, \ldots, N$ the Neumann components:

$$\Phi_\theta^N = \sin\left(\frac{i-(N+1)}{2N+3}(2\theta+1)\pi\right), \quad i = 0, \ldots, N.$$

In Figure 2 we show the Dirichlet and Neumann Fourier modes for $N = 3$. These discrete Fourier components allow us to write the solution vector $\mathbf{x} = \{\mathbf{x}_f, \mathbf{x}_S\}$ in the Fourier basis by

$$\mathbf{x}_f = \sum_{\theta_x=1}^{N}\sum_{\theta_y=1}^{N} x_f(\theta_x, \theta_y)\Phi_{\theta_x}^D\Phi_{\theta_y}^D, \quad \mathbf{x}_S = \sum_{\theta_x=0}^{N}\sum_{\theta_y=1}^{N} x_S(\theta_x, \theta_y)\Phi_{\theta_x}^N\Phi_{\theta_y}^D, \tag{18}$$

Lemma 5.1 (Eigenvalues)**.** *Let Δ_h^D be the discretization of the Laplacian in Ω_f with Dirichlet values on on $\partial\Omega_f$ and Δ_h^N be the discretization of the Laplacian in Ω_s with Neumann boundary values on Γ_i and Dirichlet boundary values on the remaining parts*

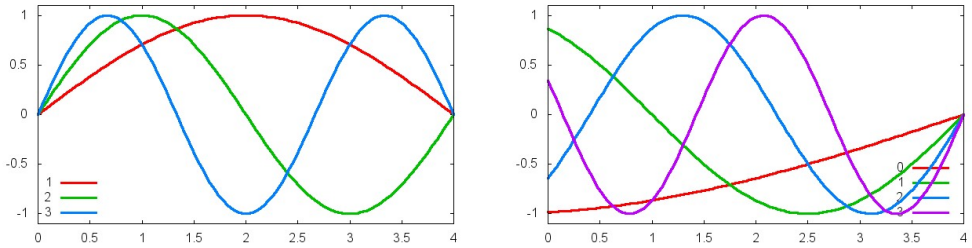

Figure 2: Fourier components for $N = 3$. Left: Dirichlet values on both sides, right: Neumann values on the left, Dirichlet on the right boundary of the domain.

of the boundary. It holds:

$$\begin{aligned}
\Delta_h^D \Phi_{\theta_x}^D \Phi_{\theta_y}^D =& \lambda^D(\theta_x,\theta_y)\Phi_{\theta_x}^D \Phi_{\theta_y}^D,\\
\lambda^D(\theta_x,\theta_y) :=& \frac{2}{3}\Big\{4 - \cos\big(\frac{\theta_x\pi}{N+1}\big) - \cos\big(\frac{\theta_y\pi}{N+1}\big) - 2\cos\big(\frac{\theta_x\pi}{N+1}\big)\cos\big(\frac{\theta_y\pi}{N+1}\big)\Big\},\\
\Delta_h^N \Phi_{\theta_x}^N \Phi_{\theta_y}^D =& \lambda^N(\theta_x,\theta_y)\Phi_{\theta_x}^N \Phi_{\theta_y}^D,\\
\lambda^N(\theta_x,\theta_y) :=& \frac{2}{3}\Big\{4 - \cos\big(\frac{(2\theta_x+1)\pi}{2N+3}\big) - \cos\big(\frac{\theta_y\pi}{N+1}\big) - 2\cos\big(\frac{(2\theta_x+1)\pi}{2N+3}\big)\cos\big(\frac{\theta_y\pi}{N+1}\big)\Big\}.
\end{aligned} \tag{19}$$

Further, the Fourier components are orthogonal and it holds:

$$\sum_{i=1}^{N} \Phi_\theta^D(i)^2 = \frac{N+1}{2}, \quad \sum_{i=0}^{N} \Phi_\theta^N(i)^2 = \frac{2N+3}{4}. \tag{20}$$

This result follows by easy calculation. See [28] for a detailed overview of Fourier techniques in the context of multigrid smoothers.

By Lemma 5.1 we can express the product of the matrices (or their inverse) with the Fourier components in terms of Eigenvalues. For high frequencies of the error (these are all frequencies with $\theta > N/2$ which are not seen on the next coarse mesh) it holds:

$$|\lambda^F(\theta_x,\theta_y)|, |\lambda^S(\theta_x,\theta_y)| \geq 2 \text{ for } \theta_x > \frac{N}{2} \text{ or } \theta_y > \frac{N}{2}. \tag{21}$$

After these preliminary introduction, we can state the central theorem:

Theorem 5.1 (Smoothing property)**.** *One step of the multigrid-smoothing iteration, Algorithm 2. reduced high frequent error parts by a fixed rate $\rho < 1/3$ (not depending on the mesh-size h).*

Proof. We proof this theorem by splitting the iteration into the two parts for fluid and solid:

(i) The fluid part. The new fluid-error $\mathbf{e}_f^{(i)}$ is given by

$$\mathbf{F}\mathbf{e}_f^{(i)} = -\mathbf{F}\mathbf{S}\mathbf{e}_s^{(i-1)}. \tag{22}$$

The equations for velocity and deformation are completely decoupled. Hence, it is sufficient to regard one of them. Then, the matrix $\mathbf{F}$ can be considered to be the Dirichlet Laplace discretization Δ_h^D. On the right hand side of (22), the matrix $\mathbf{FS}$ acts on the interface unknowns only and couples only between the interface unknowns (on the solid side) and the last column of fluid unknowns on the fluid-side, compare (17). Hence, let $\Phi_{\theta_y}^D$ be one Fourier component of the interface error $\mathbf{e}^{(i-1)}|_{\Gamma_i}$ before smoothing. Then, we can write $\mathbf{FS}$ in stencil notation as

$$\mathbf{FS} = -\frac{1}{3}\left[\begin{array}{c|c} & 1 \\ & 1 \\ & 1 \end{array}\right],$$

where by the line we denote, that the matrix only acts on entries beyond the fluid-domain. For the interface component $\Phi_{\theta_y}^D$ we get

$$\begin{aligned}(-[\mathbf{FS}]\Phi_{\theta_y}^D)_{i=N,j} &= \frac{1}{3}\left(\sin\left(\frac{j\pi\theta}{N+1}\right) + \sin\left(\frac{(j+1)\pi\theta}{N+1}\right) + \sin\left(\frac{(j-1)\pi\theta}{N+1}\right)\right) \\ &= \underbrace{\frac{1}{3}\left(1 + 2\cos\left(\frac{\pi\theta}{N+1}\right)\right)}_{\lambda^\Gamma(\theta_y)}(\Phi_{\theta_y}^D)_j, \end{aligned} \tag{23}$$

and $-([\mathbf{FS}]\Phi_{\theta_y}^D)_{i,j} = 0$ for $i = 1, \ldots, N-1$. For all high frequencies $\theta_y \geq N/2$ it holds:

$$|\lambda^\Gamma(\theta_y)| \leq \frac{1}{3} \quad \forall i = N/2 \ldots N, \tag{24}$$

This vector $-[\mathbf{FS}]\Phi_{\theta_y}$ is the right hand side of the fluid-error relation (22). We need to express this vector in the Fourier basis (18) of the fluid-domain by finding coefficients $e_f(\theta_x, \theta_y) \in \mathbb{R}$ such that:

$$\sum_{\theta_x=1}^{N} \mathbf{e}_f(\theta_x, \theta_y)\Phi_{\theta_x}^D(i) = \delta_{iN}\lambda^\Gamma(\theta_y) \quad \forall i = 1, \ldots, N.$$

Using the orthogonality of $\{\Phi_\theta^D,\ \theta = 1, \ldots, N\}$ and (20) we have

$$\mathbf{e}_f(\theta_x, \theta_y) = \frac{2\lambda^\Gamma(\theta_y)\Phi_{\theta_x}^D(N)}{N+1}.$$

Then, with the eigenvalues of the discrete Laplacian (19) we get

$$[\Delta_h^D]^{-1}[\mathbf{FS}]\Phi_{\theta_y}^D = \sum_{\theta_x=1}^{N} \frac{2\Phi_{\theta_x}^D(N)}{N+1}\lambda^F(\theta_x, \theta_y)^{-1}\lambda^\Gamma(\theta_y)\Phi_{\theta_x}^D\Phi_{\theta_y}^D. \tag{25}$$

For high frequencies of the interface error $\theta_y \geq N/2$ it holds with (21) and (24):

$$\sum_{\theta_x=1}^{N} \left|\frac{2\Phi_{\theta_x}^D}{N+1}\lambda^F(\theta_x, \theta_y)^{-1}\lambda^\Gamma(\theta_y)\Phi_{\theta_x}^D\right| \leq \sum_{\theta_x=1}^{N} \left|\frac{2}{N+1}\cdot\frac{1}{2}\cdot\frac{1}{3}\right| \leq \frac{1}{3}.$$

Hence, all error components of the new fluid error are at least reduced by a factor 3 for high frequent interface errors.

(ii) The structure part (Jacobi). Considering Jacobi coupling, the structural error is propagated by

$$\mathbf{Se}_S^{(i)} = -[\mathbf{SF}]\mathbf{e}_f^{(i-1)}.$$

On the right hand side, non-zeros only appear only in the ϕ-equation since the matrix $[\mathbf{SF}]$ acts only on the velocity unknowns, compare (17). Hence, the velocity error $\mathbf{v}_s - \mathbf{v}_s^{(i)}$ in $\mathbf{e}_S^{(i)}$ will be zero and it is sufficient to analyze the deformation part, given as the solution of the Laplace equation with Neumann data Δ_h^N.

The right hand side is similar to the corresponding one of the fluid-problem (22). The operator **FS** has the same structure as the **SF** and acts only between the interface and the first row of adjacent solid-nodes ($j = N$ in Figure 1). Assume, that $\mathbf{e}_f^{(i-1)}{}_{|i=N}$ is here given by the component $\Phi_{\theta_y}^D$. Then:

$$-[\mathbf{SF}]\Phi_{\theta_y}^D = \Big(\lambda^\Gamma(\theta_y)\Phi_{\theta_y}\ \underbrace{0\,0\,\ldots\,0}_{N}\Big). \tag{26}$$

where λ^Γ is as in (23), in particular with $|\lambda^\Gamma| \leq \frac{1}{3}$ for all high frequencies.

The structure problem has Neumann boundary values on the left part of the domain $i = 0$ and Dirichlet-values on the right part of the domain $i = N + 1$. Like in the fluid sub-problem, we need to express the right hand side (26) in the appropriate basis functions (18) and find with (20):

$$-[\mathbf{SF}]\Phi_{\theta_y}^D = \sum_{\theta_x=0}^{N} \frac{4\lambda^\Gamma(\theta_y)\Phi_{\theta_x}^N(0)}{2N+3}\Phi_{\theta_x}^N\Phi_{\theta_y}^D.$$

By using (19) for the new solid error it holds:

$$\mathbf{S}^{-1}[\mathbf{SF}]\Phi_{\theta_y}^D = \sum_{\theta_x=0}^{N} \frac{4\Phi_{\theta_x}^N(0)}{2N+3}\lambda^S(\theta_x,\theta_y)^{-1}\lambda^\Gamma(\theta_y)\Phi_{\theta_x}^N\Phi_{\theta_y}^D. \tag{27}$$

For all high frequencies of the error $\theta_y \geq N/2$ we get:

$$\sum_{\theta_x=0}^{N} \Big|\frac{4\Phi_{\theta_x}^N(0)}{2N+3}\lambda^S(\theta_x,\theta_y)^{-1}\lambda^\Gamma(\theta_y)\Phi_{\theta_x}^N\Big| \leq \sum_{\theta_x=0}^{N} \Big|\frac{4}{2N+3}\cdot\frac{1}{2}\cdot\frac{1}{3}\Big| \leq \frac{1}{3}.$$

Considering a Jacobi coupling we find the theorem proven with

$$\rho_J \leq \frac{1}{3}.$$

(iii) The structure part (Gauss-Seidel). If the smoother is set up in a Gauss-Seidel type by reusing the solution of the fluid-problem for the solid-problem, we need to extract

the right hand side for the solid-problem from (25). The error in the last column $i = N$ of the fluid domain is:

$$(\mathbf{F}^{-1}[\mathbf{FS}]\Phi^D_{\theta_y})_{i=N} = \sum_{\theta_x=1}^{N} \frac{2(\Phi^D_{\theta_x}(N))^2}{N+1}\lambda^F(\theta_x,\theta_y)^{-1}\lambda^\Gamma(\theta_y)\Phi^D_{\theta_y}.$$

Then, the forthcoming error on the interface gets

$$\mathbf{S}^{-1}[\mathbf{SF}]\mathbf{F}^{-1}[\mathbf{FS}]\Phi^D_{\theta_y} = \left(\sum_{\theta_x^N=0}^{N} \frac{\Phi^N_{\theta_x^N}(0)^2}{\lambda^S(\theta_x^N,\theta_y)}\right)\left(\sum_{\theta_x=1}^{N} \frac{\Phi^D_{\theta_x}(N)^2}{\lambda^F(\theta_x,\theta_y)}\right)\frac{8\lambda^\Gamma(\theta_y)^2}{(N+1)(2N+3)}.$$

With $|\Phi^D| \leq 1$, $|\Phi^N| \leq 1$ and $|\lambda^S(\theta_x,\theta_y)| \geq 2$ and $|\lambda^F(\theta_x,\theta_y)| \geq 2$ for $\theta_y \geq N/2$ the reduction rate is estimated to be

$$\frac{N+1}{2}\cdot\frac{N}{2}\cdot\frac{8}{(N+1)(2N+3)}|\lambda^\Gamma(\theta_y)|^2 \leq |\lambda^\Gamma(\theta_y)|^2 \leq \frac{1}{9},$$

resulting in the reduction rate

$$\rho_{GS} \leq \frac{1}{9}.$$

This completes the proof. □

Even though this analysis only considers a simplified set of equations, the typical coupling mechanism from fluid-structure interaction problems is present.

In this analysis we have assumed, that the matrices $\mathbf{F}$ and $\mathbf{S}$ are inverted exactly instead of approximating by the block-ILU iteration. However we know, that the block-ILU iteration is an optimal smoother for these two subproblems and high frequent error contributions are damped by a fixed rate. By $\widetilde{\mathbf{F}}^{-\nu}$ we denote ν steps of the block-ILU iteration applied to the fluid-problem. Then, for all high frequent error modes $\Phi_{\theta_x}\Phi_{\theta_y}$ it holds:

$$\left|(\mathbf{F}^{-1} - \widetilde{\mathbf{F}}^{-\nu})\Phi_{\theta_x}\Phi_{\theta_y}\right| \leq cq^\nu|\Phi_{\theta_x}\Phi_{\theta_y}|,$$

with some $q < 1$ independent on h for high frequencies. By inserting this approximate inverse in (25) and (27), we get additional error contributions which are easily controlled by choosing some $\nu > \nu_0$.

6 Numerical Examples

In this section we discuss a numerical model example: the three dimensional flow around an elastic obstacle. This example is a modification of a classic fluid-dynamics benchmark problem described by Schäfer and Turek [25]. In a domain Ω, a laminar incompressible flow is acting on an inscribed elastic body Ω_s. The body is firmly attached to parts of the boundary $\Gamma_{\text{base}} \subset \partial\Omega$ but can deform inside the domain. Aim of the benchmark problem is to identify certain values like pressure drops, drag- and lift-coefficients or the deformation of the obstacle. A similar fsi-benchmark problem has been proposed by Hron and Turek [19]. Here, also two-dimensional benchmarks based on [25] have been

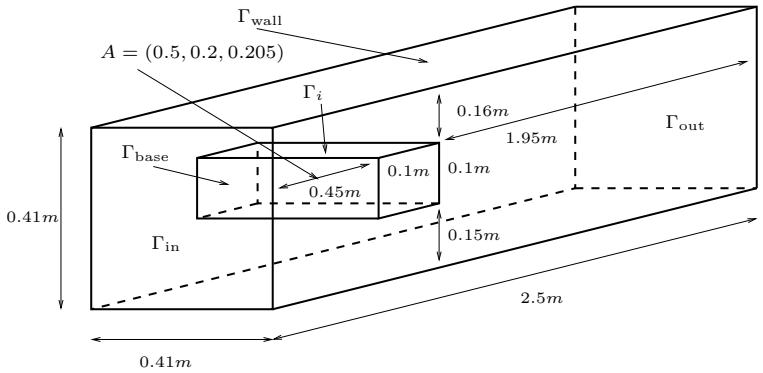

Figure 3: Configuration of the 3D fsi benchmark-problem.

elements	unknowns	$u_x(A)$	$u_y(A)$
54	4 655	$4.835 \cdot 10^{-3}$	$5.638 \cdot 10^{-5}$
432	30 303	$4.765 \cdot 10^{-3}$	$7.003 \cdot 10^{-5}$
3 456	217 175	$4.980 \cdot 10^{-3}$	$5.450 \cdot 10^{-5}$
27 648	1 641 255	$5.039 \cdot 10^{-3}$	$5.535 \cdot 10^{-5}$
221 184	12 755 015	$5.070 \cdot 10^{-3}$	$5.576 \cdot 10^{-5}$

Table 4: Deformation $u_x(A)$ and $u_y(A)$ obtained by a calculation with piecewise bi-quadratic finite elements on uniform meshes.

considered. While the two-dimensional test-cases are well suitable for direct solvers, the three-dimensional problem is by far too complex.

See Figure 3 for a sketch of the configuration. In the original benchmark-problem [25], the incompressible Navier-Stokes equations where given in the domain Ω_f, and an inflow profile was prescribed on Γ_{in}, the no-slip condition on Γ_{wall} and an outflow-condition on Γ_{out}. Here, we modify the configuration by assuming that the obstacle Ω_s is filled with an elastic material. On the boundary Γ_{base} the obstacle is fixed by a homogenous Dirichlet condition to the wall of the domain Γ_{wall}, on the inner boundary to the fluid domain Γ_i, the obstacle can freely move. Aim is to estimate the deformation in the midpoint $A = (0.5, 0.2, 0.205)$ of this deformable obstacle. On the inflow boundary Γ_{in} we prescribe a Dirichlet condition for the velocity:

$$v = 0.3 \frac{yz(0.41 - y)(0.41 - z)}{0.205^4} \quad \text{on } \Gamma_{\text{in}}.$$

On the outflow boundary Γ_{out}, the *do-nothing* condition (3) is given. On the remaining boundaries $\Gamma_{\text{wall}} \cup \Gamma_{\text{base}}$, homogenous Dirichlet conditions are given. For the deformation, we prescribe homogenous Dirichlet condition on all external boundaries $\partial\Omega$. The physical parameters are chosen as

$$\rho_f = \rho_s = 10^3, \quad \nu_f = 10^{-3}, \quad \mu_s = 10^3, \quad \lambda_s = 4 \cdot 10^3,$$

levels	# elements	# unknowns	memory	rate	steps	time
1	432	4 655	48 MB	< 0.001	1.0	< 1 s
2	3 456	30 303	213 MB	0.010	4.0	18 s
3	27 648	217 175	1 425 MB	0.039	5.0	149 s
4	221 184	1 641 255	10 803 MB	0.045	5.5	1460 s
5	1 769 472	12 755 015	85 467 MB	0.051	5.8	13270 s

Table 5: Convergence of the multigrid method for the 3D test-case: number of mesh levels, elements and unknowns. Memory usage, error reduction rate per multigrid iteration, average number of MG-iterations per Newton-cycle and average time for the solution of the linear system.

making the structure very elastic. The Reynolds number is $Re = 20$ and the Poisson ratio is $\nu_s = 0.4$. With a density ratio of $\rho_f/\rho_s = 1$ this FSI problem is strongly coupled. In Table 4 we show the results for the two output functionals, the deformation in point $A \in \Omega_s$. These results are obtained on uniform meshes using piece-wise bi-quadratic finite elements.

Next we compare the proposed multigrid solver using the splitting-smoother with the performance of a direct solver. In all calculation, piecewise tri-quadratic finite elements are used. As direct solver, the software package *MUMPS* [1] is taken. The computations have been carried out on a shared memory system without any parallelization.

Two steps of pre- and post-smoothing are taken on every level of the multigrid solver. The coarse mesh problem is solved by an exact solver. For approximating the fluid and solid sub-problem, four steps of an block-ILU preconditioned Richardson iteration are carried out. The combined effort corresponds to 8 steps of pre- and post-smoothing in a standard coupled iteration.

First, in Table 5 we show the memory consumption, multigrid convergence rates and running times on uniform meshes.

Due to the immense memory requirement of the direct solver, further simulations have been run using locally refined meshes. These meshes are adaptively created by using an energy-norm like a posteriori error estimator. In Tables 6 and 7 we compare the memory usage, running times and convergence rates (in the case of multigrid) for the two different solver, multigrid and direct.

What is approved from these calculations is the robustness of the multigrid solver. On uniform meshes in Table 5 as well as on locally refined meshes in Table 6, the convergence rates are stable and very good, at about 0.05 in every step. Memory usage grows linearly with the problem size and fairly large problems can be handled. Especially in terms of computational time, the direct solver is not competitive. On the fourth mesh with less than 5 000 quadratic elements, solution of one linear system takes nearly three hours compared to five minutes using the multigrid solver.

Finally, in Figure 4 we plot the running times and memory usage comparing the performance of the direct solver with the multigrid scheme. These numbers are taken

levels	# elements	# unknowns	memory	rate	steps	time
1	54	4 655	48 MB	< 0.001	1.0	< 1 s
2	236	17 423	144 MB	0.005	3.5	9 s
3	1 314	87 871	610 MB	0.045	5.0	65 s
4	**4 646**	**311 899**	**2 200** MB	**0.055**	**5.7**	**297** s
5	13 886	928 305	7 045 MB	0.050	5.6	854 s
6	39 338	2 596 769	21 049 MB	0.052	5.7	2552 s
7	119 432	7 850 437	63 128 MB	0.050	5.7	8156 s

Table 6: Convergence of the multigrid method for the 3D test-case on locally refined meshes: number of mesh levels, elements and unknowns. Memory usage, error reduction rate per multigrid iteration, number of iterations per Newton-cycle and time per multigrid-iteration.

levels	# elements	# unknowns	memory	time
1	54	4 655	82 MB	< 1 s
2	236	17 423	420 MB	8 s
3	1 314	87 871	3 073 MB	520 s
4	**4 646**	**311 899**	**14 089** MB	**10 688** s
5	13 886	928 305	$\sim 70\,000$ MB	$*$ s

Table 7: Convergence history of the direct solver *MUMPS* for the 3D test-case on locally refined meshes: number of mesh levels, elements and unknowns. Memory usage, time for direct solver. ($*$ the last calculation has been aborted after 48h of running time).

from Tables 6 and 7 on locally refined meshes.

All numerical simulations have been carried out with the software library *Gascoigne*, see [3].

7 Summary

We have presented a geometric multigrid solver for solving complex, three dimensional fluid-structure interaction problems in a monolithic formulation. As major source of difficulties dealing with fluid-structure interaction problems, the coupling between the two subproblems has been identified. This coupling significantly worsens the condition numbers of the system matrices as opposed to pure incompressible fluid problems or problems of elasticity.

Key of the proposed multigrid method is a splitting approach within the smoothing iteration. Here, fluid and structure problem are decoupled in a Dirichlet-Neumann type domain decomposition iteration. For a simplified equation it has been shown by Fourier analysis that this approach is suitable to damp all high frequent error of the coupled problems.

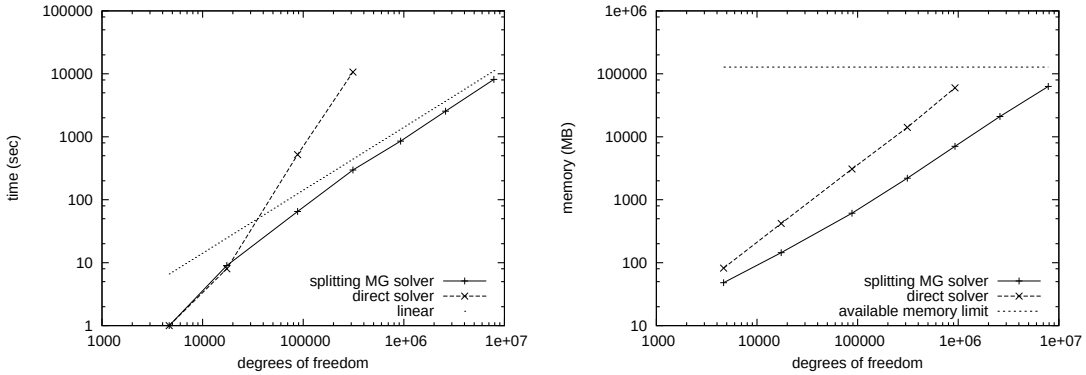

Figure 4: Comparison of the splitting multigrid solver with the direct solver *MUMPS*. Left: computational time, right memory consumption.

Finally, the multigrid method has proved its feasibility and efficiency for a three-dimensional test-case. In [22] the parallelization of the multigrid solver using the local block-structure has been demonstrated. The expansion to FSI problems and the specific splitting within the smoother is straightforward since in [22] a similar non-overlapping decomposition of the matrix is already used to construct the parallel smoother. This is subject of ongoing work.

References

[1] P. Amestoy, I. Duff, and J.-Y. L'Excellent, *Multifrontal parallel distributed symmetric and unsymmetric solvers*, Computer Methods in Applied Mechanics and Engineering, 184 (2000), pp. 501–520. doi:10.1016/S0045-7825(99)00242-X.

[2] R. Becker and M. Braack, *Multigrid techniques for finite elements on locally refined meshes*, Numerical Linear Algebra with Applications, 7 (2000), pp. 363–379. Special Issue.

[3] R. Becker, M. Braack, D. Meidner, T. Richter, and B. Vexler, *The finite element toolkit* Gascoigne. http://www.gascoigne.uni-hd.de.

[4] M. Braack and G. Lube, *Finite elements with local projection stabilization for incompressible flow problems*, Journal of Computational Mathematics, 27 (2009), pp. 116–147.

[5] M. Braack and T. Richter, *Solutions of 3D Navier-Stokes benchmark problems with adaptive finite elements*, Computers and Fluids, 35 (2006), pp. 372–392.

[6] D. Braess, *Finite Elemente*, Springer, 1997.

[7] S. Brenner and R. Scott, *The Mathematical Theory of Finite Element Methods*, Springer, Berlin-Heidelberg-New York, 1994.

[8] E. Brummelen, K. Zee, and R. Borst, *Space/time multigrid for a fluid-structure-interaction problem*, Applied Numerical Mathematics, 58 (2008), pp. 1951–1971.

[9] H.-J. Bungartz and M. Schäfer, eds., *Fluid-Structure Interaction. Modelling, Simulation, Optimisation*, vol. 53 of Lecture Notes in Computational Science and Engineering, Springer, 2006. ISBN-10: 3-540-34595-7.

[10] G. Carey and J. Oden, *Finite Elements, Computational Aspects*, vol. III, Prentice-Hall, 1984.

[11] P. Causin, J. Gereau, and F. Nobile, *Added-mass effect in the design of partitioned algorithms for fluid-structure problems*, Computer Methods in Applied Mechanics and Engineering, 194 (2005), pp. 4506–4527.

[12] T. Dunne, *Adaptive Finite Element Approximation of Fluid-Structure Interaction Based on Eulerian and Arbitrary Lagrangian-Eulerian Variational Formulations*, PhD thesis, University of Heidelberg, 2007. urn:nbn:de:bsz:16-opus-79448.

[13] C. Förster, W. Wall, and E. Ramm, *Artificial mass instabilities in sequential staggered coupling of nonlinear structures and incompressible viscous flows*, Computer methods Applied Mechanics and Engineering, 196 (2007), pp. 1278–1293.

[14] V. Girault and P.-A. Raviart, *Finite Elements for the Navier Stokes Equations*, Springer, 1986.

[15] W. Hackbusch, *Multi-Grid Methods and Applications*, Springer, 1985.

[16] M. Heil, A. Hazel, and J. Boyle, *Solvers for large-displacement fluid-structure interaction problems: Segregated vs. monolithic approaches*, Computational Mechanics, 43 (2008).

[17] J. Heywood, R. Rannacher, and S. Turek, *Artificial boundaries and flux and pressure conditions for the incompressible Navier-Stokes equations*, Int. J. Numer. Math. Fluids, 22 (1992), pp. 325–352.

[18] J. Hron and S. Turek, *A monolithic fem/multigrid solver for an ale formulation of fluid-structure interaction with applications in biomechanics*, in Fluid-Structure Interaction: Modeling, Simulation, Optimization, H.-J. Bungartz and M. Schäfer, eds., Lecture Notes in Computational Science and Engineering, Springer, 2006, pp. 146–170.

[19] ——, *Proposal for numerical benchmarking of fluid-structure interaction between an elastic object and laminar incompressible flow*, in Fluid-Structure Interaction: Modeling, Simulation, Optimization, H.-J. Bungartz and M. Schäfer, eds., Lecture Notes in Computational Science and Engineering, Springer, 2006, pp. 371–385.

[20] J. Hron, S. Turek, M. Madlik, M. Razzaq, H. Wobker, and J. Acker, *Numerical simulation and benchmarking of a monolithic multigrid solver for fluid-structure interaction problems with application to hemodynamics*, in Fluid-Structure Interaction II: Modeling, Simulation, Optimization, H.-J. Bungartz and M. Schäfer, eds., Lecture Notes in Computational Science and Engineering, Springer, 2010, pp. 197–220.

[21] A. Huerta and W. Liu, *Viscous flow with large free-surface motion*, Computer Methods in Applied Mechanics and Engineering, 69 (1988), pp. 277–324.

[22] M. Kimmritz and T. Richter, *Parallel multigrid method for finite element simulations of complex flow problems on locally refined meshes*, Numerical Linear Algebra with Applications, (2010). doi: 10.1002/nla.744.

[23] S. Piperno and C. Farhat, *Paritioned procedures for the transient solution of coupled aeroelastic problems - part ii: energy transfer analysis and three-dimensional applications*, Computer Methods in Applied Mechanics and Engineering, 190 (2001), pp. 3147–3170.

[24] T. Richter and T. Wick, *Finite elements fo fluid-structure interaction in ale and fully eulerian coordinates*, Computer Methods in Applied Mechanics and Engineering, (2010). doi: 10.1016/j.cma.2010.04.016).

[25] M. Schäfer and S. Turek, *Benchmark computations of laminar flow around a cylinder. (With support by F. Durst, E. Krause and R. Rannacher)*, in Flow Simulation with High-Performance Computers II. DFG priority research program results 1993-1995, E. Hirschel, ed., no. 52 in Notes Numer. Fluid Mech., Vieweg, Wiesbaden, 1996, pp. 547–566.

[26] S. Turek, *Efficient Solvers for Incompressible Flow Problems: An Algorithmic and Computational Approach*, Springer, 1999. ISBN 3-540-65433-X.

[27] W. Wall, *Fluid-Structure Interaction with Stabilized Finite Elements*, PhD thesis, University of Stuttgart, 1999. urn:nbn:de:bsz:93-opus-6234.

[28] R. Wienand, *Extended Local Fourier Analysis for Multigrid: Optimal Smoothing, Coarse Grid Correction and Preconditioning*, no. 20 in GMD Research Series, GMD Forschungszentrum Informationstechnik GmbH, Sankt Augustin, 2001. ISBN 3-88457-403-5.